Wobbling around the clock: magnetically-driven quasi-periodic oscillations in pulsating ultraluminous X-ray sources

M. Veresvarska, M. Imbrogno, R. Amato, G. L. Israel, S. Scaringi, 1.5

P. Casella, D. de Martino, F. Fürst, A. Gúrpide, C. Knigge, M. J. Middleton,

Accepted XXX. Received YYY; in original form ZZZ

ABSTRACT

Ultraluminous X-ray sources (ULXs) are X-ray binary systems containing an accreting neutron star (NS) or black hole emitting at luminosities above the Eddington limit of a $10\,M_\odot$ black hole. Approximately 1900 (either confirmed or candidate) ULXs have been identified to date. Three systems have been confirmed to exhibit coherent signals consistent with NS spin frequencies and quasi-periodic oscillations (QPOs) in the mHz range. Several interpretations for generating such QPOs have been proposed, including general relativistic frame-dragging effects. In this work, we test if an alternative model in which magnetically-driven precession of the inner accretion flow can self-consistently reproduce the observed NS spin and QPO frequencies for reasonable values for accretion rates and NS magnetic field strengths. For a range of parameters, we recover family of solutions with accretion rates $\approx 10^{-7}$ – $10^{-5}\,M_\odot$ yr $^{-1}$ and surface magnetic fields $\gtrsim 10^{12}\,G$, in agreement with previous estimates. If validated, this interpretation could reconcile several observed properties of pulsating ULXs, including QPO frequencies and the observed high luminosities of these systems, in a self-consistent framework without requiring general relativistic effects and/or strong beaming due to specific viewing angles. Although the predictive power of the model is currently limited by parameter degeneracies and uncertainties, searching for and discovering more pulsating ULX systems will allow to further test or refute the proposed model.

Key words: accretion, accretion discs – stars: neutron – magnetic fields – X-rays: binaries – X-rays: individual: M82 X-2, M51 ULX-7, NGC 7793 P13

1 INTRODUCTION

Ultraluminous X-ray sources (ULXs) are a class of X-ray binaries with luminosities $L_{\rm X}\gtrsim 10^{39}\,{\rm erg\,s^{-1}}$, exceeding the Eddington limit ($L_{\rm Edd}\simeq 1.3\times 10^{38} M/M_{\odot}\,{\rm erg\,s^{-1}}$, with M being the mass of the accretor) of a $\sim 10\,{\rm M}_{\odot}$ black hole (BH; see Kaaret et al. 2017; Fabrika et al. 2021; King et al. 2023; Pinto & Walton 2023, for recent reviews). First detected by the *Einstein Observatory* in the off-nuclear regions of nearby galaxies (Fabbiano 1989), they have been proposed to be possible intermediate-mass black hole (IMBH) candidates with $M_{\rm BH}\simeq 10^2-10^6\,{\rm M}_{\odot}$, accreting at sub-Eddington rates (see e.g. Colbert & Mushotzky 1999). The presence of mHz quasi-periodic oscillations (QPOs) in some ULXs (see e.g. Strohmayer et al. 2007; Strohmayer & Mushotzky 2009; Pasham et al. 2015; Atapin et al. 2019), interpreted as the low-frequency counterparts of QPOs in

Galactic BH binaries (van der Klis 1989), seemingly supported this hypothesis. Indeed, using the mass-frequency scaling derived from Galactic BH binaries (e.g. Aschenbach 2004; Remillard & McClintock 2006; Smith et al. 2018), the masses inferred from the QPO frequencies are found to be in the IMBH range (see e.g. Casella et al. 2008 and Figure 4 of Smith et al. 2018). However, some differences cast doubt on such simple analogies. For example, in the case of Galactic BH binaries, the QPO frequency $\nu_{\rm QPO}$ tightly correlates with a low frequency break $\nu_{\rm b}$, with $\nu_{\rm QPO}\approx 10\nu_{\rm b}$ (Wijnands & van der Klis 1999). Such a correlation is not observed in ULXs with QPOs (see e.g. Middleton et al. 2011).

The detection in a few ULXs of coherent pulsations with $P \sim 0.1-10\,\mathrm{s}$ – known as pulsating ULXs (PULXs) – has demonstrated that at least some of these sources are powered instead by neutron stars (NSs) accreting at super-Eddington rates (King et al. 2001; Poutanen et al. 2007; Zampieri & Roberts 2009). A few of these PULXs also show mHz QPOs at super-Eddington luminosities, providing additional evidence that care is needed when using the QPO frequency in a (P)ULX to estimate the mass of the accretor. A total of 12 (either

¹Department of Physics, Centre for Extragalactic Astronomy, Durham University, South Road, Durham DH1 3LE, UK

²Dipartimento di Fisica, Università degli Studi di Roma "Tor Vergata", via della Ricerca Scientifica 1, I-00133 Rome, Italy

³INAF – Osservatorio Astronomico di Roma, via Frascati 33, I-00078 Monte Porzio Catone (RM), Italy

⁴Dipartimento di Fisica, Università degli Studi di Roma "La Sapienza", piazzale Aldo Moro 5, I-00185 Roma, Italy

⁵INAF – Osservatorio Astronomico di Capodimonte, Salita Moiariello 16, I-80131 Naples, Italy

⁶European Space Astronomy Centre (ESAC), ESA, Camino Bajo del Castillo s/n, Villanueva de la Cañada, E-28692 Madrid, Spain

⁷School of Physics and Astronomy, University of Southampton, Highfield, Southampton SO17 1BJ, UK

^{*} E-mail: martina.veresvarska@durham.ac.uk

[†] These authors contributed equally.

[‡] E-mail: matteo.imbrogno@inaf.it

confirmed or candidate) PULXs have been discovered (see Table 2 of King et al. 2023), with luminosities up to $\sim 10^{41}$ erg s⁻¹ (Israel et al. 2017a). How these sources can reach such high luminosities is still unclear, with some arguing that the inferred luminosities (derived under the isotropic emission approximation) could be overestimated due to geometrical beaming (see e.g. King et al. 2017; Lasota & King 2023).

In this paper, we focus on those PULXs that have shown mHz QPOs at (observed) luminosities $\geq 10^{39} \, \mathrm{erg \, s^{-1}}$: M82 X-2 (Feng et al. 2010), M51 ULX-7 (Imbrogno et al. 2024) and NGC 7793 P13 (Imbrogno et al., in prep.). M82 X-2 was the first source identified as a PULX (Bachetti et al. 2014). With a luminosity $L_{\rm X} \simeq 10^{39}$ – $10^{40} \, \mathrm{erg \, s^{-1}}$ and an orbital period $P_{\mathrm{orb}} \simeq 2.5 \, \mathrm{d}$, the NS powering M82 X-2 is found near spin equilibrium, with a spin period $P \simeq$ 1.37 s. The source alternates between strong spin-up and spin-down phases over the years, despite less drastic changes in luminosity, and shows a spin evolution inconsistent with that expected from a slow rotator, as shown by Bachetti et al. (2020). M82 X-2 is also a good example of how the estimate of the mass of the accretor in a ULX from the QPO frequency can be misleading. The nature of the accretor was unknown when Feng et al. (2010) detected a QPO at $v \simeq 3$ mHz in a few Chandra observations, leading the authors to conclude that the source was a good IMBH candidate, with $M \simeq 12000 - 43000 \,\mathrm{M}_{\odot}$, \sim four orders of magnitude larger than the real mass $(M \simeq 1.4 \, \mathrm{M}_{\odot})$.

M51 ULX-7, whose spin pulsations at $P \simeq 2.8$ s were first detected by Rodríguez Castillo et al. (2020), is the PULX with the shortest known orbital period ($P_{\rm orb} \simeq 2$ d; Hu et al. 2021; Vasilopoulos et al. 2021). It is also characterised by a super-orbital modulation, initially detected with a period $P_{\rm so} \simeq 38$ d, but later found to be gradually evolving towards a longer period $P_{\rm so} \simeq 45$ d (Brightman et al. 2020; Vasilopoulos et al. 2020; Brightman et al. 2022). Recently, Imbrogno et al. (2024) detected a flaring-like feature in the light curve of three *XMM-Newton* observations of the source. A Fourier analysis of these data revealed the presence of a QPO at a frequency $v \simeq 0.5$ mHz. The same feature was detected also in *Chandra* archival observations. In both sources, the QPO is always present at the same frequency (Imbrogno et al. 2024).

Lastly, NGC 7793 P13 is the fastest known PULX, with a spin period $P \simeq 0.4$ s (Fürst et al. 2016; Israel et al. 2017b). It is the only PULX with an identified optical counterpart (Motch et al. 2011). A peculiarity of this system is that the orbital periods estimated through optical ($P_{\rm opt} \simeq 64$ d) and X-ray ($P_{\rm X} \simeq 65$ d) are not compatible, an inconsistency which remains without a clear explanation (Fürst et al. 2018, 2021). Recently, a QPO at $v \simeq 10$ mHz was detected in a few *XMM-Newton* observations of NGC 7793 P13 (Imbrogno et al., in prep.). As for M51 ULX-7, the QPO is always found at a specific frequency and only when the system emits at super-Eddington luminosities.

Various models have been proposed to explain the presence of mHz QPOs in (P)ULXs. Middleton et al. (2019) proposed that mHz QPOs arise from a precessing inner flow of the disc. The general relativistic frame-dragging torque (inducing Lense-Thirring precession) is then communicated to the launched winds, whose precession is expected to cause the much longer super-orbital period seen in many (P)ULXs (see e.g. Kong et al. 2016; Walton et al. 2016; Fürst et al. 2018; Vasilopoulos et al. 2020; Brightman et al. 2020, 2022). Atapin et al. (2019), instead, proposed that the propagating fluctuations mechanism from Lyubarskii (1997) can explain both the QPO and the flat-topped noise observed in a sample of ULXs. Majumder et al. (2023) followed Das et al. (2021) to link the QPO frequency to the infall time towards the inner radius of the disc, and hence proposing to use the QPO frequency to infer the masses of the cen-

tral object, assumed to be a BH. A similar mechanism for generating quasi-periodic variability, but for NSs, is also explored in Mushtukov et al. (2024).

Contrary to BHs, the presence of a magnetosphere and its dynamical importance to the accretion flow in PULXs can be substantial and is expected to exert additional torques on the inner flow. The effect of the magnetosphere through what we refer to here as the magneticallydriven precession model (MDP model hereafter) has been explored for both magnetised NSs and T Tauri stars by Lai (1999) and more recently for accreting white dwarfs (WDs) by Veresvarska et al. (2024). In this paper, we explore the validity of applying the MDP model, presented in Sect. 2, to the mHz QPOs recently detected in a few PULXs. In particular, we want to verify if the MPD model can simultaneously match the spin and QPO periods observed in these PULXs for reasonable values of the accretion rate and the magnetic field. With this goal in mind, we apply the model to the PULXs showing QPOs and present the results in Sect. 3. Finally, we discuss the implications of our results, together with the strengths and limitations of the model in Sect. 4.

2 MAGNETIC PRECESSION MODEL

The MDP model can in principle generate QPOs from magnetically driven precession, where the accretion flow surrounding a rotating magnetised star experiences a quasi-periodic wobbling motion around the star's spin axis. The interaction between the disc and the star's magnetic field induces a warping effect, causing the inner flow to deviate from its equatorial plane and to undergo precession. This precessing motion is driven by the torque that arises from the interaction between the misaligned disc's surface currents to the star's magnetic field, generated by its dipole, in the plane of the accretion disc

The MDP model further explores the non-linear evolution of the warped disc, as detailed by Pfeiffer & Lai (2004). The application of this model to low-frequency QPOs in NSs is also examined in Shirakawa & Lai (2002a,b). Within this framework the global precession of the disc can generate the observed QPOs, offering insights into the underlying mechanisms driving these oscillations in various accreting systems, including WDs and NSs.

Lai (1999) estimates the precession frequency of the entire inner flow by scaling the magnetic precession frequency of a specific ring at a characteristic radius, r, $v_p(r)$, with a dimensionless constant A. The value of the constant A depends on the disc structure. Shirakawa & Lai (2002a,b) estimate A in the range 0.3–0.85 and here we fix this to a fiducial value of 0.65 (close to the midpoint of the quoted range). This leads to the expression for the QPO frequency:

$$\nu_{\rm QPO} = A\nu_p(r) = \frac{A}{2\pi^3} \frac{\mu^2}{r^7 \Omega(r) \Sigma(r)} \frac{F(\theta)}{D(r)},\tag{1}$$

where μ represents the stellar magnetic dipole moment ($\mu = BR^3$, with B as the surface magnetic field strength and R the stellar radius), Ω is the Keplerian angular frequency, and Σ is the surface density of the disc (here assumed to be represented by Equation 5.41 in (Frank et al. 2002)) as adopted for the NS application of the MDP model in Lai (1999); Shirakawa & Lai (2002b).

The dimensionless function $F(\theta)$ is defined such that $F(\theta) = 2f\cos^2\theta - \sin^2\theta$, where θ is the angle between the magnetic moment of the accretor and the angular momentum of the disc. The dimensionless number $f(0 \le f \le 1)$ determines what part and how much of the vertical magnetic field is being screened out; here, we take f = 0 as in Pfeiffer & Lai (2004); Veresvarska et al. (2024), so

that only the spin-variable vertical field is screened out (for f = 1 all the vertical field is screened out). D(r) is a dimensionless function given by

$$D(r) = \max\left(\sqrt{\frac{r^2}{r_{\rm in}^2} - 1}, \sqrt{\frac{2H(r)}{r_{\rm in}}}\right),$$
 (2)

where H(r) is the half-height of the disc at radius r and $r_{\rm in}$ is the magnetospheric radius from Eq. 4. In the first applications to NS in Lai (1999); Shirakawa & Lai (2002b) and the WD application in Veresvarska et al. (2024) of the MDP model the disc half-height is assumed from Equation 5.41 in Frank et al. (2002). Here we retain this height prescription. The overall sub-Eddington treatment of the model here is anchored in the assumption that $r_{\rm M} > r_{\rm sph}$, where $r_{\rm sph}$ is the spherisation radius, defined as the radius at which the inflow starts to be supercritical (Poutanen et al. 2007) and $r_{\rm M}$ is the magnetospheric radius.

An alternative half height prescription which could lead to exploration of the model within the spherisation radius is detailed in (Lipunova 1999). Compared to the thin disc prescription, the steeper dependence of disc height on accretion rate results in a $\frac{H}{R} \sim 1$ at $\dot{M} \sim 10^{-6} - 10^{-5} M_{\odot} yr^{-1}$ for a 1.4 M_{\odot} NS with 10 km radius. This prescription for the half-height of the disc in Lipunova (1999) results in the inverse dependence of QPO frequency on accretion rate as opposed to the direct dependence for a thin-disc prescription. However, implementation of the super-Eddington regime would also require further changes to the model, namely in the surface density and the condition of $r_{\rm M} < r_{\rm sph}$. Exploration of this implementation is the subject of future work and beyond the scope of this paper.

Table 1 lists all the parameters adopted in this study together with the explored ranges, where some are set to fixed fiducial values. Although some of the parameter ranges can be constrained from the work of Chashkina et al. (2017, 2019) (where $\alpha \sim 0-0.2$ for M82 X-2), we here explore all parameter ranges given in Table 1 for completeness.

In order to reduce several parameter degeneracies, we here assume spin equilibrium such that the co-rotation ($r_{\rm co}$) and magnetosphere ($r_{\rm M}$) radii are equal. This is a reasonable assumption in the case of M82 X-2, as already discussed in the Introduction, while it comes with some caveats for NGC 7793 P13 and M51 ULX-7, which are currently spinning up (see Fürst et al. 2021, 2025; Brightman et al. 2022 and the Discussion). Assuming spin equilibrium, we can anchor the QPO radius to the spin and magnetic field, reducing the degeneracy between them. Thus, $r = r_{\rm M} = r_{\rm co}$, where the co-rotation radius is defined as:

$$r_{\rm co} = \left(\frac{GMP_{\rm spin}^2}{4\pi^2}\right)^{\frac{1}{3}},\tag{3}$$

where $P_{\rm spin}$ is the spin period of the NS, M its mass and G the gravitational constant. Similarly, the magnetospheric radius is here defined as:

$$r_{\rm M} = \eta \left(\frac{2\pi^2}{\mu_0^2} \frac{\mu^4}{GM\dot{M}^2} \right)^{\frac{1}{7}},\tag{4}$$

where μ_0 is the vacuum permeability. η is generally assumed to be 0.5 (Wang 1987; Ghosh & Lamb 1979; Campana et al. 2018), however a wider range of values (Table 1) are explored here. Implications of this assumption on the model are further discussed in Section 4.

A parameter of the MDP model is the mass accretion rate $\dot{M}_{\rm acc}$ onto the compact object, which can differ from the mass loss rate from the donor star through the L1 point (see Section 4). We can

Table 1. Model parameters for the magnetically driven precession model for QPOs in NS XRBs. Parameters with their explored ranges are given. For some cases they are fixed to a fiducial value, where only that one is given and denoted by *.

Model Parameter	Value
$\mathrm{M}^*\left(M_\odot\right)$	1.4
R* (km)	10
B (G)	$10^8 - 10^{15}$
$\dot{M} (M_{\odot} yr^{-1})$	$10^{-10} - 10^{-3}$
α	$10^{-3} - 1$
η	$10^{-2} - 1$
θ (°)	0 - 90
A*	0.65

obtain a rough estimate of $\dot{M}_{\rm acc}$ through the gravitational energy released assuming most is emitted at X-ray wavelengths:

$$\dot{M}_{\rm acc} = \frac{2bR_{\rm NS}L_{\rm obs}}{GM_{\rm NS}} \tag{5}$$

where b is the beaming factor (such that b=1 corresponds to no beaming), $L_{\rm obs}$ is the observed isotropic luminosity of the source, $M_{\rm NS}$ and $R_{\rm NS}$ are the mass and radius of the NS. Note that the $L_{\rm obs}$ does not distinguish between the luminosity of the different components of the system (i.e. accretion disc, winds, etc.), but represents the observed luminosity as an upper limit. Furthermore, the linear relation between accretion rate and luminosity is used, as opposed to Equation 4 in (Middleton et al. 2023), since within the framework of the assumptions made here, it is expected that $r_{\rm M} > r_{\rm sph}$. In such cases super-Eddington accretion can be sustained for high magnetic field strengths (Gúrpide et al. 2021).

3 RESULTS

We apply the model described in Section 2 and explore the parameter space as detailed in Table 1 to three PULXs, namely M82 X-2, M51 ULX-7 and NGC 7793 P13, for which both the spin and QPO periods have been detected.

The parameter space in Table 1 presents a wide array of combinations leading to a family of solutions with the same QPO and spin. To explore this non-linear parameter space and recover families of solutions that can reproduce the observed spin and QPO frequencies, we first generate 108 model realisations using parameter combinations randomly drawn from a flat distribution in log space (apart from θ as the range spans fewer orders of magnitude than the other parameters) within the ranges given in Table 1. We then retain those parameter combinations for which both the model-predicted QPO and spin are within the 1σ errors of their measured values as reported in Table 2. In the case of M82 X-2, where several QPO measurements exist, we take the average of the individual QPO measurements from Table 1 of Feng et al. (2010). In the case of M51 ULX-7, the QPO was fitted with two separate Lorentzians in Imbrogno et al. (2024). Here we assume that the Lorentzian at lower frequency with larger $Q = \frac{v}{\Delta v} \ge 2.1$ is the QPO, whilst the higher frequency Lorentzian corresponds to the "broad component". Finally, in the case of NGC 7793 P13 we found that one Lorentzian was enough to model the QPO (Imbrogno et al., in prep.) and we took the average value of the QPO frequency.

The model realisations (under the assumption of no beaming i.e. b = 1) which reproduced the QPO frequencies and spin periods

Table 2. List of observational parameters present in literature and the B field inferred form the MDP model, for the three PULXs considered in this work

Source	References	P _{spin} (s)	ν _{QPO} (mHz)	$-\dot{M}_{\star}$ (10 ⁻⁷)	$\dot{M}_{\rm acc}/b$ $M_{\odot} {\rm yr}^{-1})$	b	B _{MDP} (10 ¹³ G)
M82 X-2	[1,2,3]	1.32-1.39	2.77-3.98	47(2)	20-40 2-4	1 0.1	> 0.8 > 0.3
M51 ULX-7	[4,5,6]	2.79-3.28	0.53-0.56	_ _	5-12 0.5-1.2	1 0.1	> 2 > 0.7
NGC 7793 P13	[7,8,9,10]	0.406-0.420	11-15	- -	5-8 0.5-0.8	1 0.1	> 0.3 > 0.1

Notes. Reference values for $P_{\rm spin}$, $\nu_{\rm QPO}$ and (in the case of M82 X-2) $\dot{\rm M}_{\star}$, the overall mass-transfer rate from the companion, taken from: [1] Feng et al. (2010); [2] Bachetti et al. (2022); [3] Liu (2024); [4] Rodríguez Castillo et al. (2020); [5] Imbrogno et al. (2024); [6] Earnshaw et al. (2016); [7] Fürst et al. (2016); [8] Israel et al. (2017b); [9] Fürst et al. (2021); [10] Imbrogno et al. (in prep). The reported values of the mass-accretion rate \dot{M}_{acc} for b=1 have been inferred from the X-ray luminosities (typically in the 0.3-10 keV band) of the datasets where QPOs have been detected.

within their errors are shown in Figure 1 for M82 X-2 and in Figure A1 and A2 for M51 ULX-7 and NGC 7793 P13 respectively, as grey points. Figures 1, A1 and A2 show a corner plot displaying a parameter sweep through all combinations.

We first consider the case of M82 X-2, since it is also the only PULX for which an estimated measurement mass-transfer rate from the donor star (\dot{M}_{\star}) has been inferred from the derivative of the orbital period (Bachetti et al. 2022) (although note King & Lasota (2021) associate this signal to stochastic variability). Assuming the orbital period derivative is indeed driven by the mass-transfer rate from the donor, we can reduce the number of family of solutions that can reproduce the QPO and spin of M82 X-2. The red diamonds in Figure 1 represent another set of model realisations in which all parameters are randomly drawn from flat distributions as for the grey points, but are additionally constrained by a uniform distribution within the range of \dot{M}_{\star} in Table 2. With this additional constrain a correlation between B and η is observed, where lower B requires higher η (Figure 1). A similar relation is found between B and \dot{M} , where higher \dot{M} provides reasonable constraints for higher B, when not considering the \dot{M} constraint from Table 2. Therefore, limiting \dot{M} for M82 X-2 yields a smaller set of family of solutions with a lower limit on $B \gtrsim 1 \times 10^{13}$ G. Furthermore the observed X-ray luminosity can be explained with no beaming with the assumed mass accretion rate. Nevertheless, we show in Table 2 the effects on the recovered B field assuming a moderate beaming of b = 0.1. We also explored the effects of moderate beaming, likely due to the geometry of the inner part of the accretion disk and the presence of a wind component often observed in ULXs (Middleton et al. 2015; Pinto et al. 2016; Pinto & Kosec 2023). It is worth noting that the MDP model does not directly include beaming but only mass accretion rate. Thus in producing the red points in Figure 1, b is set to the minimum luminosity required to justify the observed \dot{P} . The effect of varying the beaming factor (for b = 0.1) is shown by the blue diamonds in Figures A1 and A2. This has the effect of lowering the required accretion rate (see Eq. 5), which allows for a factor ≈ 3 lower B fields. The other parameters remain largely unaffected. In either case, the dipolar magnetic field B is found to be larger than 10^{12} G for all three sources.

4 DISCUSSION AND CONCLUSIONS

The magnetic torque exerted by the NS on the accretion disc generates a precession of the innermost regions, potentially giving rise to the observed mHz QPOs. Other torques have been invoked to explain these QPOs, as well as the superorbital periodicities observed in several ULXs. For instance, the Lense-Thirring precession model has been applied to the non-pulsating NGC 5408 X-1, to interpret both its QPOs and time lags (Middleton et al. 2019). Other possible mechanisms that can induce precession are asymmetries in the NS with respect to its spin axis (free-body precession, Jones & Andersson 2001), magnetic or self-induced warping (Lai 2003; Pfeiffer & Lai 2004; Pringle 1996), tidal torque from the donor star (Frank et al. 2002) and warping of an inclined disc due to the relativistic Bardeen-Petterson effect (Bardeen & Petterson 1975). Two or more of these mechanisms could in principle be competing. This would explain, for instance, the presence of (magnetically-induced) QPOs and superorbital periods observed in all three PULXs discussed in this work. Middleton et al. (2018) discussed the relative strengths of magnetic and Lense-Thirring torques in ULXs, concluding that the magnetic torque would be negligible for $B \sim 10^{10-11}$ G and $\alpha \sim 0.01$. However, for larger B, as considered here (Table 2) and larger α , the magnetic torque is expected to be more dominant and becomes a viable option for generating QPOs. Another relativistic effect that can be present concurrently with magnetic warping is the Bardeen-Patterson effect (Bardeen & Petterson 1975; King et al. 2005; Ingram & Motta 2019). In such a case, an inner tilted disc is warped towards the orbital plane of the system at similar scales as the Lense-Thirring precession. However, a lower limit on the QPO frequency caused by this effect can be set at ~ 3 Hz (Fragile et al. 2001). This is significantly higher than the frequencies of the QPOs reported in this work in Table 2, making it unlikely that the Bardeen-Petterson effect and the magnetically induced warp can counteract one another on the same scale size in the disc.

Despite the complexity of the phenomena that can generate QPOs, in this work we focussed on the effects of a misaligned NS magnetic field to the accretion disc (MDP model) and recovered reasonable family of solutions. In the following Sections, we discuss and outline the most important aspects and limitations of the model when applied to the QPOs in PULXs (Section 4.1), the effects of beaming on the accretion rate of the systems, the implications on the preferred model parameters (Section 4.2), the implications of the model on the properties of the PULXs, as well the potential avenues for identifying

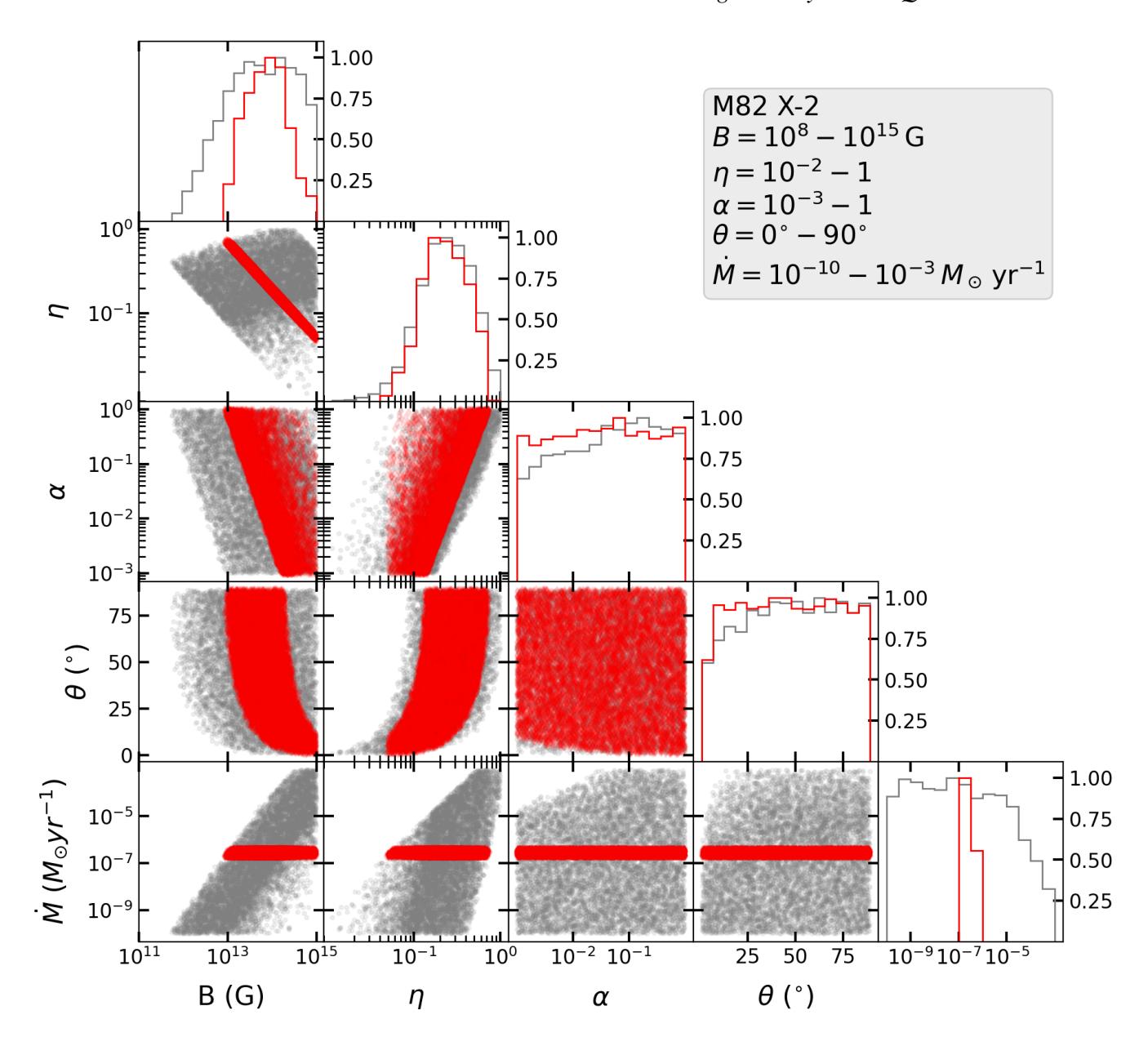


Figure 1. Parameter space of the MDP model with all parameter combinations (in grey circles) producing QPO frequency and spin within the observed errors as noted in Table 2. All the solutions which also reproduce accretion rate within the range given by the observed \dot{P} are given in red diamonds. Distributions of all parameters are provided, with all being scaled to unity. The explored parameter ranges are noted as also shown in Table 1.

future candidates of mHz QPOs that can test the MDP model further (Section 4.3).

4.1 Limitations of the model

Given the number of free parameters in Table 1 any conclusions drawn from the model application should be treated with caution. Apart from the lack of direct observational evidence for the viability of the inferred parameters, it is also important to discuss other assumptions used by the model. One of them is the systems are in spin-equilibrium, such that $r = r_{\rm in} = r_{\rm M} = r_{\rm co}$. This is not necessarily the case for any system with an observed secular spin-up or spin-down (Fürst et al. 2021). By analogy however, accreting WDs that are thought to be in spin-equilibrium do display both

spin-up and/or spin-down around the equilibrium point (Patterson et al. 2020). Nonetheless, the adopted spin-equilibrium assumption adopted here conveniently removes several parameter degeneracies. As already mentioned, this assumption is likely correct only by M82 X-2 at present - but crucially not when the QPOs were detected.

We further note that the model is very sensitive to parameters α and θ , whose combinations are degenerate in all ULXs as seen in Figures 1, A1 and A2. As shown in Figure 1 for M82 X-2, high accretion rates rule out low viscosity α and low angles θ .

The MDP model is also very sensitive to changes in η . However constraining the mass accretion rate significantly constrains η . The standard value of $\eta \sim 0.5$ used in literature for magnetic accretors (Wang 1987; Ghosh & Lamb 1979; Campana et al. 2018) is used as the fiducial value and reproduces reasonable results, for $\alpha \gtrsim 0.1$ and

B on the lower end of the range given in Table 2 for most systems. However M82 X-2 has been reported to be out of spin-equilibrium during some of the QPO measurements (Liu 2024). It is thus not surprising that families of solutions with $\eta < 0.5$ can reproduce the observed accretion rate in Table 2.

Similarly, NGC 7793 P13 is known to be out of spin-equilibrium (see the long-term evolution of the spin period discussed by Fürst et al. 2021 and Fürst et al. 2025). Following the example of M82 X-2, $\alpha \sim 0.1-0.2$ would require setting $\eta \sim 0.3$ to reproduce the observed accretion rates $\dot{\rm M}_{\rm acc}/b$, well below the observational limit for the mass loss of the known donor (see below). Naturally, a higher value of α would then also allow for $\eta = 0.5$.

The present model does not take into account all key aspects of super-Eddington accretion physics (e.g. Shakura & Sunyaev 1973; Poutanen et al. 2007), but it is interesting nonetheless that it can recover reasonable families of solutions. For a NS accreting at super-Eddington rates, the magnetospheric radius, $r_{\rm M}$, is usually smaller than $r_{\rm sph}$, depending on the magnetic field strength and accretion rate, as also shown in numerical simulations (Chashkina et al. 2017, 2019), also inferred from the application of the MDP model to the three considered PULXs. Using the equation for spherisation radius from Poutanen et al. (2007) and the measured spin periods of the 3 PULXs considered here, the spherisation radii for the sources considered here are $\sim 990~R_{\rm g}, \sim 165~R_{\rm g}$ and $\sim 330~R_{\rm g}$ for M82 X-2, M51 ULX-7 and NGC 7793 P13 respectively, with R_g being the gravitational radius. However the associated magnetospheric radii based on the observed spins and $r_{\rm M} = r_{\rm CO}$ are $\sim 990~R_{\rm g}, \sim 1700$ $R_{\rm g}$ and $\sim 450~R_{\rm g}$ for M82 X-2, M51 ULX-7 and NGC 7793 P13 respectively. This suggests that $r_{\rm M} \sim r_{\rm sph}$ only for M82 X-2. For M51 ULX-7 and NGC 7793 P13 $r_{\rm M} > r_{\rm sph}$, as also suggested by Gúrpide et al. (2021) for high magnetic fields. This would imply the model applied here is self-consistent, at least for M51 ULX7 and NGC 7793 P13 and justifies our assumption of ignoring mass-loss.

4.2 Beaming factor

The MDP model requires a mass accretion rate, which can be converted to an observed luminosity assuming a beaming factor (Eq. 5). As already discussed in Section 3, beaming is likely present and should be considered. Whether this beaming is moderate or extreme is still a matter of debate (see e.g. Israel et al. 2017a and King & Lasota 2020 for both scenarios).

For M82 X-2, strong beaming is not required to reconcile the observed X-ray luminosity with the mass accretion rate inferred by Bachetti et al. (2022) through the secular orbital period derivative $\dot{P}_{\rm orb}$. In the case of M51 ULX-7 and NGC 7793 P13, the available X-ray data do not allow a \dot{P}_{orb} measurement, and therefore an estimate of \dot{M}_{\star} . However, the latter can be inferred from the observed luminosity, as $L_{\text{obs}} = L_{\text{acc}}/b$. Some recent observational results suggest that if the beaming is present, it should be relatively small (see e.g. Israel et al. 2017a; Rodríguez Castillo et al. 2020). This is also the case for another PULX, NGC 5907 ULX-1, for which a luminosity of 10⁴¹ erg s⁻¹ has been inferred from its surrounding nebula, suggesting that it is a genuine super-Eddington accretor with no need of (strong) beaming (Belfiore et al. 2020). Additionally, the morphology and strength of He II, H β and [O I] emission regions in the nebula surrounding Ho II X-1 and NGC 1313 X-1 strongly argue against the presence of extreme beaming (Kaaret et al. 2004; Gúrpide & Castro Segura 2024). Moreover, the inferred mass-transfer from the companion $\dot{M}_{\rm orb}$ in M82 X-2 shows that the mass available for accretion onto the NS is $\sim 150 \, M_{\odot} \text{yr}^{-1}$, high enough to account for the observed luminosity (100 times the Eddington limit) without invoking (strong) beaming (Bachetti et al. 2022). Finally, as already emphasised, strong beaming would imply a too small torque on the NS to account for the observed \dot{P} . Because of this we explored moderate beaming factors (>1/10), resulting in a reduction of the predicted B field by about a factor of \sim 4. For M82 X-2 and M51 ULX-7 this still poses a lower limit on the $B \gtrsim 10^{13}$ G within the MDP model assumptions and $B \gtrsim 10^{12}$ G for NGC 7793 P13.

4.3 Implications of the model and future perspectives

As discussed in Section 4.1, the MDP model is based on the standard accretion theory for an optically thick, geometrically thin disc (Shakura & Sunyaev 1973), with a modification for the disc thickness to mimic a supercritical accretion disc, but without taking into account any further element specific to super-Eddington accretion (winds, thick disc, radiation pressure, etc.). When applied to the sample of PULXs, the model yields reasonable families of solutions with mass-accretion rates, spin and QPO frequencies consistent with those obtained from observations. Within the recovered families of solutions, the inferred dipolar magnetic fields are found to be between a few 10¹² G and a few 10¹³ G, also consistent with the literature estimates (Fürst et al. 2016; Israel et al. 2017b; Rodríguez Castillo et al. 2020; Bachetti et al. 2022), and of the same order of magnitude to the known X-ray pulsars in HMXBs in our Galaxy and in the Magellanic Clouds.

A potential implication of the MDP model may be the transitional behaviour of QPOs and spin pulses in M51 ULX-7, where the QPO is observed when the spin signal is absent and vice versa, without significant spectral variations in the source (see Imbrogno et al. 2024 for details). Within the MDP model, this may suggest that the tilted, precessing inner flow could partially or fully obscure the neutron star's accretion column. In this case, large values of θ would cause a drop in pulse coherence, while when $\theta \sim 0$, the alignment minimises obscuration, leading to increased pulse coherence and the absence of QPOs, due to the inner disc symmetry. It is worth clarifying that while the lack of spin pulses is attributed to the precession of the inner disc, θ relates to the tilt of the outer parts of the disc (Veresvarska et al. 2024). This suggests that the outer disc may also precess to some extent, potentially influencing the overall dynamics of the system, as noted in Imbrogno et al. (2024). A more detailed investigation of how the outer and inner disc regions interact and contribute to observed variability could provide further insights into the coupling between QPOs, spin pulses, and disc precession.

Further implication arises from the expected observational correlations depending on the assumed disc half-height prescription. As mentioned above, assuming a thin disc from Shakura & Sunyaev (1973) yields a positive correlation between the QPO frequency and the accretion rate. On the other hand, the disc half-height prescription more appropriate for a geometrically thick ULX inner disc (Lipunova 1999) yields a negative correlation. Therefore, with sufficient data on a given QPO in different states, the QPO frequency is expected to change based on the underlying accretion rate, with the variations being driven by the type of inner accretion flow. A QPO with a nonvarying frequency throughout different states would thus rule out the MDP model. However, such data is not available, with M51 ULX-7 showing very little variation in QPO frequency over ~ 10 year period where state changes have not been observed (Imbrogno et al. 2024).

In principle, the MDP model could provide a direct way to estimate the magnetic field strength from the QPO and spin frequencies. However, the dependence on other unconstrained model parameters (α, θ) and accretion rate) make this challenging. Despite this, new

Atapin K., Fabrika S., Caballero-García M. D., 2019, MNRAS, 486, 2766

and independent measurements of the magnetic field strength, could lead to a new method to constrain η and potentially α .

Furthermore, with M82 X-2 in spin equilibrium and based on the assumptions that spin equilibrium implies $\eta \sim 0.5$ and $r_{\rm M} \sim r_{\rm CO}$, the MDP model predicts that the QPO should move to lower frequencies for the same spin and accretion rate ($\sim 5 \times 10^{-4}$ Hz assuming the viscosity remains unchanged).

Of all the analysed PULXs, NGC 7793 P13 is the only one with a known companion star (B9Ia class, Motch et al. 2014). The estimated mass-loss rate of the star can be as high as $\sim 10^{-5} \ \mathrm{M_{\odot} \, yr^{-1}}$ (El Mellah et al. 2019). Adopting this value as an upper limit on the mass-transfer rate in ULXs, we can place limits on the expected spin period and magnetic field strength of other candidate PULXs showing mHz QPOs. As an example, 2CXOJ140314.3+541816 (Urguhart et al. 2022) and 4XMMJ111816.0-324910 (Motta et al. 2020) have been suggested to host accreting NSs due to a hard spectrum and large variation in the luminosity, respectively. Using the same model set-up and adopting the fiducial parameters from Table 1, we explore the family of solutions adopting the strict upper limit for the mass-transfer rate of \dot{M} <10⁻⁵ M_{\odot} yr⁻¹. For the QPO in 2CXOJ140314.3+541816 at 1.35-1.92 mHz we infer $0.5 \text{ ms} \lesssim P_{\text{spin}} \lesssim 8 \text{ s and } B > 3 \times 10^9 \text{ G}$, consistent with the previously suggested $B \sim 10^{10} \text{G}$ and $P_{\text{spin}} \sim 5 \text{ms}$ (Urquhart et al. 2022). Similarly for 4XMMJ111816.0-324910 we infer $0.5 \text{ ms} \lesssim P_{\text{spin}} \lesssim 4 \text{ s}$ and $B \sim 10^{10} \text{G}$ for QPO frequency $\sim 0.3 \text{ mHz}$. We note that these limits only pertain to the specific case of the fiducial parameters from Table 1. Nevertheless, assuming the magnetically driven precession model as the mHz QPO driver suggests a spin period range for potential new pulsation detections. Obtaining new independent measurements of the dipolar magnetic field of the NSs could help remove some of the degeneracies in the model. This could then potentially open up an avenue of independent constraint on the elusive nature of viscosity α .

ACKNOWLEDGEMENTS

MI is supported by the AASS Ph.D. joint research programme between the University of Rome "Sapienza" and the University of Rome "Tor Vergata", with the collaboration of the National Institute of Astrophysics (INAF). MV acknowledges the support of the Science and Technology Facilities Council (STFC) studentship ST/W507428/1. SS is supported by STFC grant ST/T000244/1 and ST/X001075/1. RA and GLI acknowledge financial support from INAF through grant "INAF-Astronomy Fellowships in Italy 2022 - (GOG)". GLI also acknowledge support from PRIN MUR SEAWIND (2022Y2T94C) funded by NextGenerationEU and INAF Grant BLOSSOM. DdM acknowledges support from INAF through "Astrofisica Fondamentale 2022 - Large grant N.16

DATA AVAILABILITY

The data analysed in this article are public and can be downloaded from the *XMM-Newton* Science Archive XSA (http://nxsa.esac.esa.int/nxsa-web/#search) and the High Energy Astrophysics Science Archive Research Center (HEASARC) archive (https://heasarc.gsfc.nasa.gov/cgi-bin/W3Browse/w3browse.pl).

```
REFERENCES
```

Aschenbach B., 2004, A&A, 425, 1075

Bachetti M., et al., 2014, Nature, 514, 202

```
Bachetti M., et al., 2020, ApJ, 891, 44
Bachetti M., et al., 2022, ApJ, 937, 125
Bardeen J. M., Petterson J. A., 1975, ApJ, 195, L65
Belfiore A., et al., 2020, Nature Astronomy, 4, 147
Brightman M., et al., 2020, ApJ, 895, 127
Brightman M., et al., 2022, ApJ, 925, 18
Campana S., Stella L., Mereghetti S., de Martino D., 2018, A&A, 610, A46
Casella P., Ponti G., Patruno A., Belloni T., Miniutti G., Zampieri L., 2008,
    MNRAS, 387, 1707
Chashkina A., Abolmasov P., Poutanen J., 2017, MNRAS, 470, 2799
Chashkina A., Lipunova G., Abolmasov P., Poutanen J., 2019, A&A, 626,
Colbert E. J. M., Mushotzky R. F., 1999, ApJ, 519, 89
Das S., Nandi A., Agrawal V. K., Dihingia I. K., Majumder S., 2021, MNRAS,
    507, 2777
Earnshaw H. M., et al., 2016, MNRAS, 456, 3840
El Mellah I., Sundqvist J. O., Keppens R., 2019, A&A, 622, L3
Fabbiano G., 1989, ARA&A, 27, 87
Fabrika S. N., Atapin K. E., Vinokurov A. S., Sholukhova O. N., 2021,
    Astrophysical Bulletin, 76, 6
Feng H., Rao F., Kaaret P., 2010, ApJ, 710, L137
Fragile P. C., Mathews G. J., Wilson J. R., 2001, ApJ, 553, 955
Frank J., King A., Raine D. J., 2002, Accretion Power in Astrophysics: Third
    Edition
Fürst F., et al., 2016, ApJ, 831, L14
Fürst F., et al., 2018, A&A, 616, A186
Fürst F., et al., 2021, A&A, 651, A75
Fürst F., Walton D. J., Bachetti M., Earnshaw H., Brightman M., 2025,
    Astronomische Nachrichten, 346, e20240106
Ghosh P., Lamb F. K., 1979, ApJ, 234, 296
Gúrpide A., Castro Segura N., 2024, MNRAS, 532, 1459
Gúrpide A., Godet O., Koliopanos F., Webb N., Olive J. F., 2021, A&A, 649,
Hu C.-P., Ueda Y., Enoto T., 2021, ApJ, 909, 5
Imbrogno M., et al., 2024, A&A, 689, A284
Ingram A. R., Motta S. E., 2019, New Astron. Rev., 85, 101524
Israel G. L., et al., 2017a, Science, 355, 817
Israel G. L., et al., 2017b, MNRAS, 466, L48
Jones D. I., Andersson N., 2001, MNRAS, 324, 811
Kaaret P., Ward M. J., Zezas A., 2004, MNRAS, 351, L83
Kaaret P., Feng H., Roberts T. P., 2017, ARA&A, 55, 303
King A., Lasota J.-P., 2020, MNRAS, 494, 3611
King A., Lasota J.-P., 2021, arXiv e-prints, p. arXiv:2112.03779
King A. R., Davies M. B., Ward M. J., Fabbiano G., Elvis M., 2001, ApJ,
King A. R., Lubow S. H., Ogilvie G. I., Pringle J. E., 2005, MNRAS, 363, 49
King A., Lasota J.-P., Kluźniak W., 2017, MNRAS, 468, L59
King A., Lasota J.-P., Middleton M., 2023, New Astron. Rev., 96, 101672
Kong A. K. H., Hu C.-P., Lin L. C.-C., Li K. L., Jin R., Liu C. Y., Yen D.
    C.-C., 2016, MNRAS, 461, 4395
Lai D., 1999, ApJ, 524, 1030
Lai D., 2003, ApJ, 591, L119
Lasota J.-P., King A., 2023, MNRAS, 526, 2506
Lipunova G. V., 1999, Astronomy Letters, 25, 508
Liu J., 2024, ApJ, 961, 196
Lyubarskii Y. E., 1997, MNRAS, 292, 679
Majumder S., Das S., Agrawal V. K., Nandi A., 2023, MNRAS, 526, 2086
Middleton M. J., Roberts T. P., Done C., Jackson F. E., 2011, MNRAS, 411,
Middleton M. J., Walton D. J., Fabian A., Roberts T. P., Heil L., Pinto C.,
    Anderson G., Sutton A., 2015, MNRAS, 454, 3134
Middleton M. J., et al., 2018, MNRAS, 475, 154
```

```
Middleton M. J., Fragile P. C., Ingram A., Roberts T. P., 2019, MNRAS, 489,
    282
Middleton M., Gúrpide A., Walton D. J., 2023, MNRAS, 519, 2224
Motch C., Pakull M. W., Grisé F., Soria R., 2011, Astronomische Nachrichten,
Motch C., Pakull M. W., Soria R., Grisé F., Pietrzyński G., 2014, Nature, 514,
    198
Motta S. E., et al., 2020, ApJ, 898, 174
Mushtukov A. A., Ingram A., Suleimanov V. F., DiLullo N., Middleton M.,
    Tsygankov S. S., van der Klis M., Portegies Zwart S., 2024, MNRAS,
Pasham D. R., Cenko S. B., Zoghbi A., Mushotzky R. F., Miller J., Tombesi
    F., 2015, ApJ, 811, L11
Patterson J., et al., 2020, ApJ, 897, 70
Pfeiffer H. P., Lai D., 2004, ApJ, 604, 766
Pinto C., Kosec P., 2023, Astronomische Nachrichten, 344, e20220134
Pinto C., Walton D. J., 2023, arXiv e-prints, p. arXiv:2302.00006
Pinto C., Middleton M. J., Fabian A. C., 2016, Nature, 533, 64
Poutanen J., Lipunova G., Fabrika S., Butkevich A. G., Abolmasov P., 2007,
    MNRAS, 377, 1187
Pringle J. E., 1996, MNRAS, 281, 357
Remillard R. A., McClintock J. E., 2006, ARA&A, 44, 49
Rodríguez Castillo G. A., et al., 2020, ApJ, 895, 60
Shakura N. I., Sunyaev R. A., 1973, A&A, 24, 337
Shirakawa A., Lai D., 2002a, ApJ, 564, 361
Shirakawa A., Lai D., 2002b, ApJ, 565, 1134
Smith K. L., Mushotzky R. F., Boyd P. T., Wagoner R. V., 2018, ApJ, 860,
Strohmayer T. E., Mushotzky R. F., 2009, ApJ, 703, 1386
Strohmayer T. E., Mushotzky R. F., Winter L., Soria R., Uttley P., Cropper
    M., 2007, ApJ, 660, 580
Urquhart R. T., et al., 2022, MNRAS, 511, 4528
Vasilopoulos G., Lander S. K., Koliopanos F., Bailyn C. D., 2020, MNRAS,
    491, 4949
Vasilopoulos G., Koliopanos F., Haberl F., Treiber H., Brightman M., Earn-
    shaw H. P., Gúrpide A., 2021, ApJ, 909, 50
Veresvarska M., et al., 2024, MNRAS, 534, 3087
Walton D. J., et al., 2016, ApJ, 827, L13
Wang Y. M., 1987, A&A, 183, 257
Wijnands R., van der Klis M., 1999, ApJ, 514, 939
Zampieri L., Roberts T. P., 2009, MNRAS, 400, 677
van der Klis M., 1989, ARA&A, 27, 517
```

APPENDIX A: MAGNETIC PRECESSION MODEL PARAMETER SPACE FOR M51 ULX-7 AND NGC 7793 P13

This paper has been typeset from a TEX/IATEX file prepared by the author.

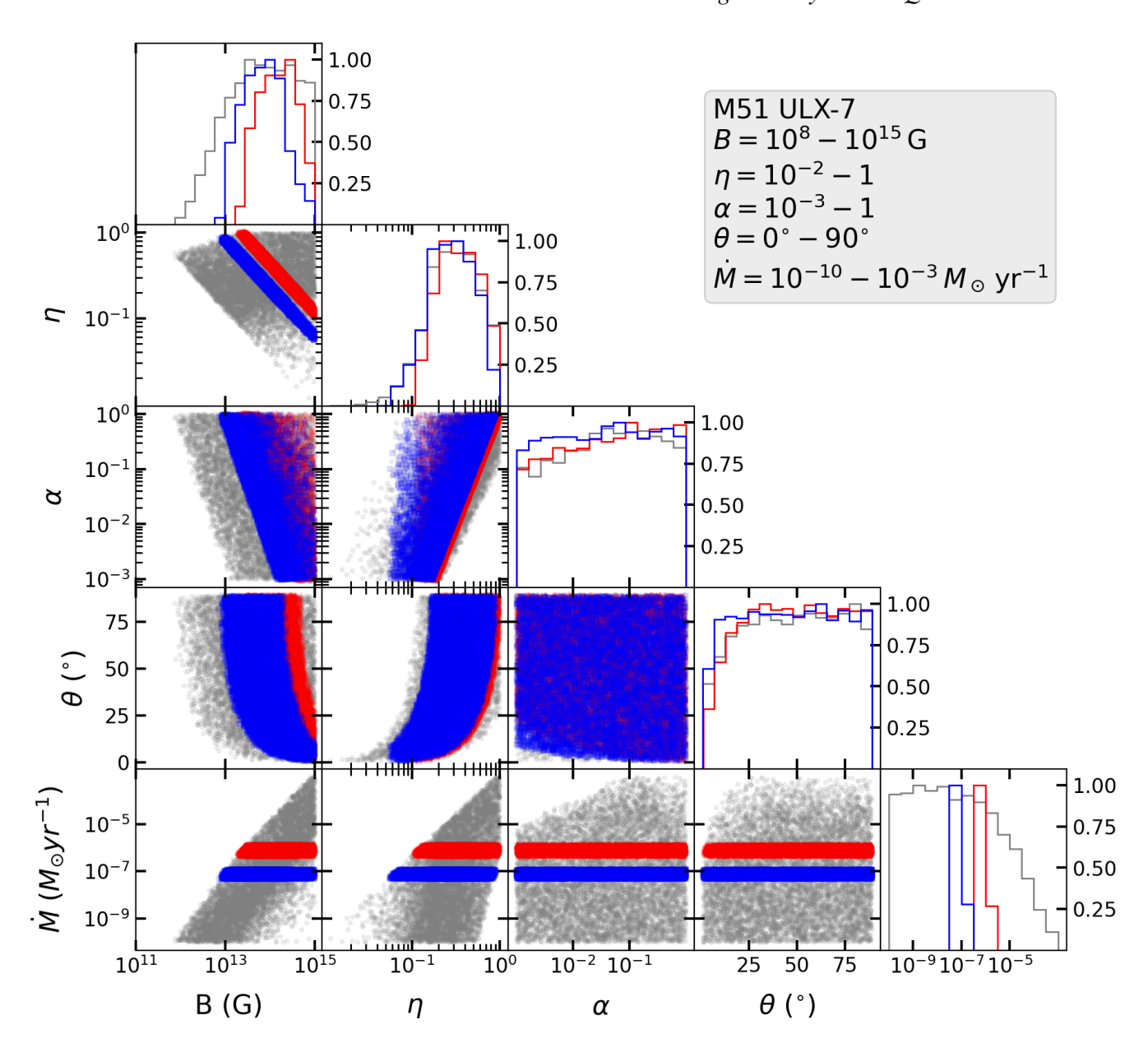


Figure A1. Parameter space of the MDP model for M51 ULX-7 with all parameter combinations (in grey circles) producing QPO frequency and spin within the observed errors as noted in Table 2. All the solutions which also reproduce accretion rate within the range in Table 2 are given in red diamonds for no beaming (b = 1) and in blue squares for moderate beaming of b = 0.1. Distributions of all parameters are provided, with all being scaled to unity. The explored parameter ranges are noted as also shown in Table 1.

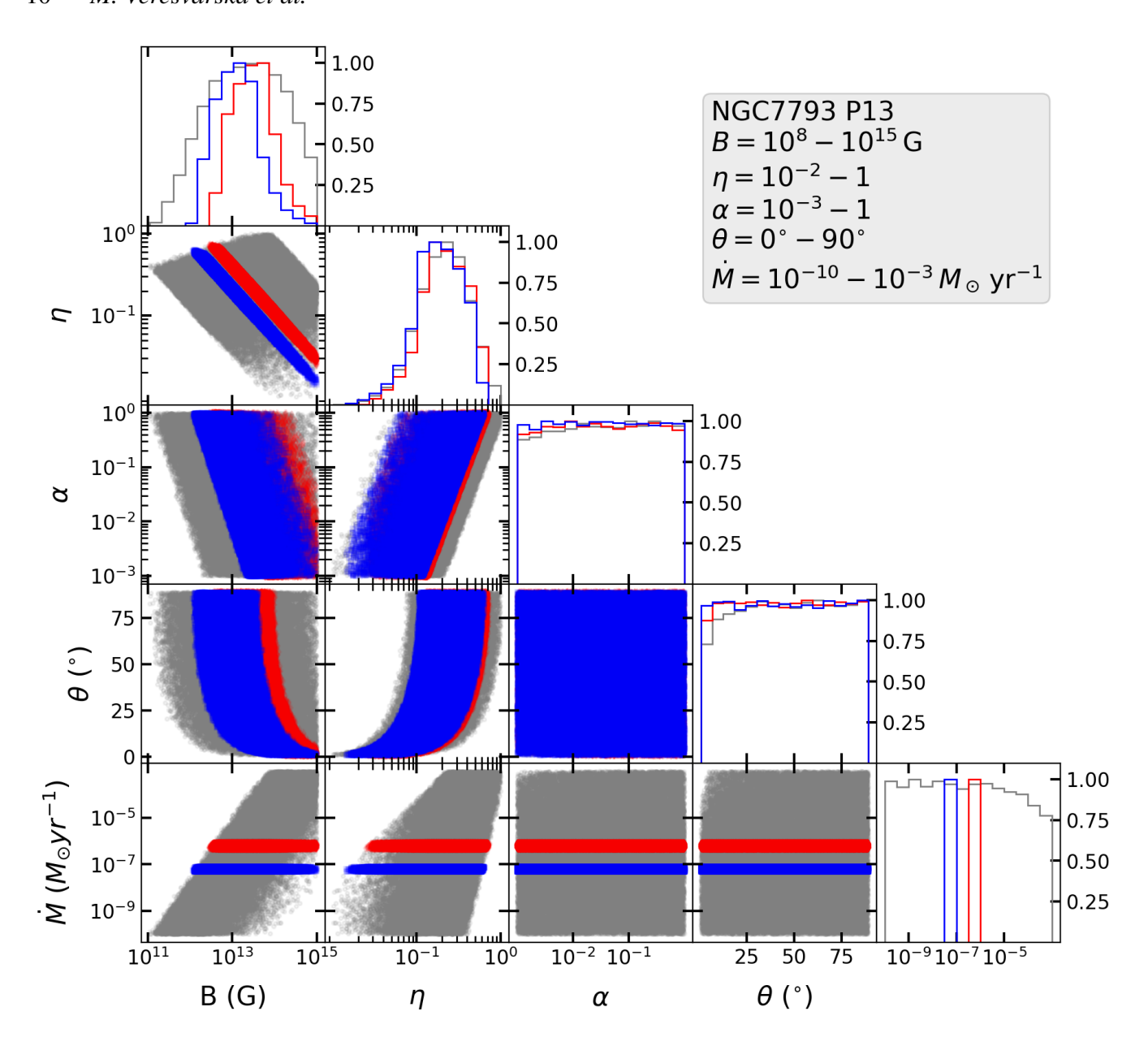


Figure A2. Parameter space of the MDP model for NGC 7793 P13 with all parameter combinations (in grey circles) producing QPO frequency and spin within the observed errors as noted in Table 2. All the solutions which also reproduce accretion rate within the range in Table 2 are given in red diamonds for no beaming (b = 1) and in blue squares for moderate beaming of b = 0.1. Distributions of all parameters are provided, with all being scaled to unity. The explored parameter ranges are noted as also shown in Table 1.